Lensless Ultra-Miniature CMOS Computational Imagers and Sensors

David G. Stork and Patrick R. Gill
Computational Sensing and Imaging
Rambus Labs
1050 Enterprise Way, Suite 700
Sunnyvale, CA 94089 USA

***Abstract*—We describe a new class of lensless, ultra-miniature computational imagers and image sensors employing special optical phase gratings integrated with CMOS photodetector matrices. Because such imagers have no lens, they are ultra-miniature ($\sim$100 μm), have large effective depth of field (1 mm to infinity), and are very inexpensive (a few Euro cents). The grating acts as a two-dimensional visual "chirp" and preserves image power throughout the Fourier plane (and hence preserves image information); the final digital image is not captured as in a traditional camera but instead computed from raw photodetector signals. The novel representation at the photodetectors demands that algorithms such as deconvolution, Bayesian estimation, or matrix inversion with Tikhonov regularization be used to compute the image, each having different bandwidth, space and computational complexities for a given image fidelity. Such imaging architectures can also be tailored to extract application-specific information or compute decisions (rather than compute an image) based on the optical signal. In most cases, both the phase grating and the signal processing can be optimized for the information in the visual field and the task at hand. Our sensor design methodology relies on modular parallel and computationally efficient software tools for simulating optical diffraction, for CAD design and layout of gratings themselves, and for sensor signal processing. These sensors are so small they should find use in endoscopy, medical sensing, machine inspection, surveillance and the Internet of Things, and are so inexpensive that they should find use in distributed network applications and in a number of single-use scenarios, for instance in military theaters and hazardous natural and industrial conditions.**

Keywords: Computational sensing, phase grating, diffractive imager, application-specific sensing

I. Introduction

The traditional *camera obscura* model—in which each point in the scene is imaged onto a single point on a sensor or image plane—has dominated the science and technology of imaging systems for several millennia, at least for sources illuminated by incoherent light. The Chinese philosopher Mo Ti traced an inverted image produced by a pinhole camera to record an image in the fifth century B.C. [1] and Johannes Kepler traced a real image projected by a converging lens onto paper in 1603. Chemical recording of projected images, such as by mercury or silver halide, was invented in 1826 and the first true digital camera was built in 1975, [2] all these exploiting the fundamental camera obscura architecture.

The rise in digital imaging, where image processing can be incorporated into the data chain, has enabled new imaging architectures. Cathey and Dowski took an early and conceptually important step away from the traditional camera obscura model by exploiting digital processing [3]. They designed a cubic-phase optical plate which, when inserted into the optical path of a traditional camera, led to an image whose (significant) blur was independent of the object depth: the image on the sensor plane did not "look good" as it would in a traditional camera obscura. Subsequent image processing sharpened the entire blurred image, thus leading to enhanced depth of field. Since then the field of *computational imaging* has explored imaging architectures in which the raw signals do not superficially resemble a traditional image; instead, the final image is computed from such signals. More and more of the total imaging "burden" is borne by computation, thereby expanding the class of usable optical components. In this way, many optical aberrations can be corrected computationally rather than optically. This imaging paradigm has led to new conceptual foundations of joint design of optics and image processing, [4] as well as a wide range of non-standard imaging architectures such as plenoptic, coded-aperture and multi-aperture systems, each with associated methods of signal processing [5]–[9].

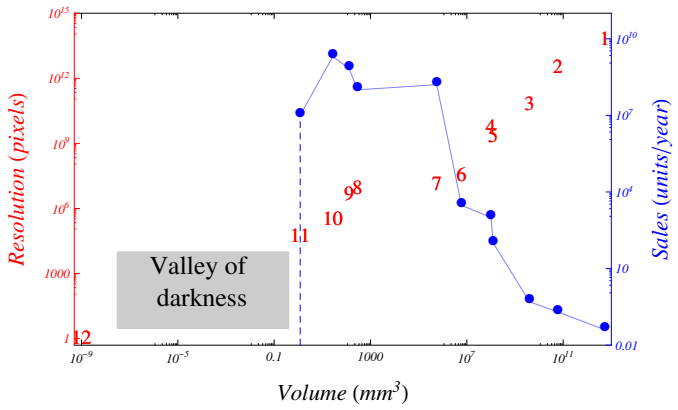

Fig. 1. The left ordinate axis in red shows the resolution (in pixels) versus the physical volume (in mm^3) of representative lens- and mirror-based telescopes and cameras (log-log scale). Notice there is a seven-order-of-magnitude range in physical volume devoid of such cameras (the **Valley of darkness**). 1 Grand Canaria telescope, 2 Hubble telescope, 3 1-m telescope, 4 30-cm telescope, 5 AWARE 2 camera, 6 Professional camera,7 Consumer DSLR, 8 iPhone 5 camera, 9 Pelican camera, 10 Miniature VGA, 11 Medigus camera, 12 Single photodiode (without lens). The right ordinate axis in blue indicates the sales of representative imagers of different physical volumes in units/year worldwide in 2013. (The unit sales figures are estimates based on historical data and market reports and do not include research prototypes and unreleased products.) Note that there is a precipitous drop in sales at the Valley of darkness. Our lensless integrated diffraction grating/CMOS imagers lie within this "valley."

The economic pressures for miniaturization of electronic devices, including cameras, arising in the mobile computing

market have led to smaller imager form factors [10]. Figure 1 shows the resolution, in total pixels per exposure, versus physical volume of imaging systems in the traditional camera obscura architecture (or curved mirror equivalent). While such imagers span 22 orders of magnitude in physical volume and 15 orders of magnitude in pixel resolution, the smaller the imager the greater the number sold commercially... but only down to a scale of roughly 1 mm^3. There is a conspicuous gap of seven orders of magnitude in physical volume—the "Valley of darkness"—between the smallest digital camera and a single unlensed photoreceptor. It seems that the camera obscura model has reached its physical limits and cannot be scaled much smaller. A new imaging architecture is required to span the Valley of darkness.

Recently, a new miniature imaging architecture has been explored, one based on integrating optics with CMOS photodetectors [11]–[15]. In brief, this architecture forgoes lenses and relies instead on simple square-wave diffraction gratings created in CMOS itself. The earliest designs in this architecture relied on CMOS wires to act as amplitude optical grating patches, the gratings producing a wavelet-like representation of the scene on the sensor matrix. More recently, square-wave *phase* gratings have also been explored [16]. For a given image resolution, such diffractive elements enable the construction of imagers much smaller than does the basic camera obscura model. (We mention in passing that related CMOS structures have been explored for integrated spectroscopy as well [17].)

There are a number of limitations of such previous work. First, amplitude gratings based on CMOS wires have poor low-light sensitivity because most of the incident light never strikes the photodetector. Second, regular diffraction gratings are by their very nature wavelength sensitive, i.e., the pattern of light on the photodetectors depends strongly upon the wavelength of incident light. Third, such imagers are sensitive to manufacturing defects—specifically a small deviation in the thickness of the grating layer can lead to a large (and difficult to correct) alteration of the diffraction pattern on the photodetectors [13].

The method we describe here, while based on integrated silicate phase optics and CMOS image sensors, is fundamentally different from prior work in a number of deep ways. Our method relies on novel special phase anti-symmetric spiral phase gratings, which overcome prior limitations and afford new functionality [18]. Moreover, our new sensor architecture enables the construction of new classes of ultra-miniature sensors whose output is an estimation of some property of the scene (e.g., visual motion) or a decision (e.g., face detection or barcode reading).

We begin in Section II with a discussion of our fundamental technology and turn in Section III to a short description of our software design and analysis tools. We describe our first hardware devices in Section IV. We mention a few application areas for such sensors and imagers in Section V and conclude in Section VI with a brief summary and suggestions for future research. The results of our hardware verification of the theory and design will be presented at a later date.

II. Sensor Optics and Technology

The following description of our sensor technology follows the data path—from target source through diffractive optics to photodetector to digital signal processing to final digital image.

A. Optics of one-dimensional phase anti-symmetric gratings

The fundamental optical elements employed by our sensors are based on a new type of phase grating having phase antisymmetry. Figure 2 shows a cross section through a UV-curable acrylate binary phase grating, here specified by three free parameters, w_0, w_1 and w_2 [19]. (Generalizations to more free parameters and multiple thicknesses are straightforward.) Consider point **P** lying on the grating's plane of odd symmetry. Light from each position on one side of the plane is cancelled via destructive interference by light from the symmetric position on the other side of the plane because those waves arrive out of phase. Note that such cancellation occurs regardless of the vertical depth of **P**. As such, all points along the red dashed line are dark; we call this plane an "optical curtain" or simply "curtain" [20]. Note especially that the location of the curtain on the sensor matrix below does not change despite manufacturing errors in overall grating thickness. Finally, as the angle of incidence of the light changes, the curtains tip by the same angle (Fig. 3).

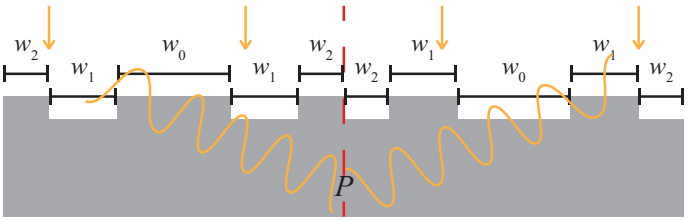

Fig. 2. A cross section through a silicate binary phase anti-symmetric phase grating, where the plane of odd symmetry is marked with a dashed red line. The parameters w_0, w_1 and w_2 describe the surface profile. For the medium's index of refraction n, the step height is chosen to corresponds to optical phase delay of π radians along the red dashed line or "curtain." For such a phase anti-symmetic grating, curtains exist even if the incident light is not normal (Figs. 3 and 4).

B. Phase anti-symmetric spiral gratings

The scenes we seek to image are two-dimensional and therefore the one-dimensional phase anti-symmetric grating and photosensor array just described must be generalized to two dimensions. Moreover, two-dimensional gratings must include segments at every orientation so as to sample the Fourier domain uniformly (and possess no zeros) and thereby enable computational reconstruction of the image from sensor responses. Figure 5 shows two examples of basic spiral grating tiles—having four-fold and six-fold chiral symmetry. These spiral grating tiles are constructed by sweeping one-dimensional phase anti-symmetric gratings perpendicularly along the length of each spiral arm. The phase anti-symmetric gratings are lengthened and made more complicated (use more ws) to cover the full tile area and feasible Fourier domain. Both spiral gratings pass information at all orientations and spatial frequencies up to the Nyquist limit, and can be tiled to cover a full photodetector matrix of arbitrary area (Fig. 6) [18]. In

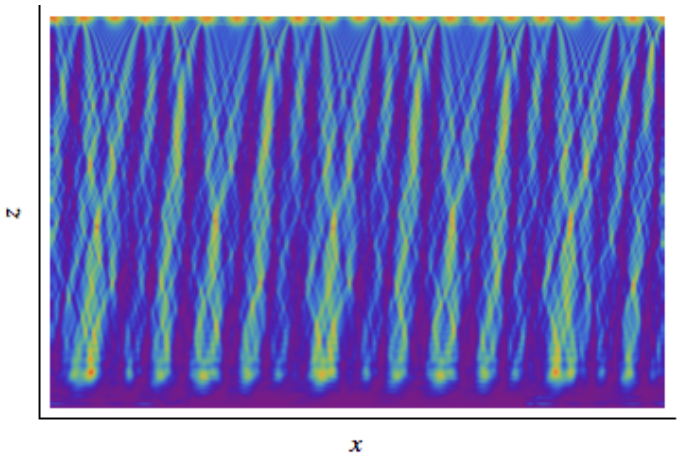

Fig. 3. A finite-difference wave simulation of the electric field energy density for monochromatic light incident at 3.5° passing through an phase anti-symmetric grating where x denotes the position left-to-right and z the depth within the silicate medium. The curtains lie beneath the points of odd symmetry (purple) and are tipped at the same angle as the incident light. Such curtains are invariant to the wavelength of incident light. The photodetector matrix (not shown) lies along the bottom.

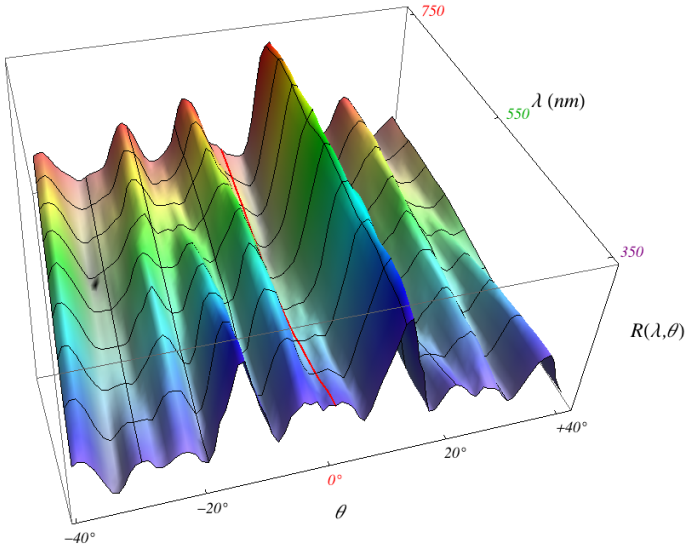

Fig. 4. The response of a single photodetector (pixel) beneath a phase anti-symmetric grating (such as **P** in Fig. 2) as a function of angle of incident light, θ, and wavelength of light, λ. Notice that for normally incident light ($\theta = 0°$) the response nearly vanishes at all wavelengths and that at each incident orientation, the response is nearly invariant with respect to wavelength. The specific form of this response function depends upon the profiles of the grating (described by w_is), which can be tailored to extract information most appropriate to particular applications, including non-imaging applications.

actual sensors, incident light covers an area at least as large as that of a full individual tile element.

The wave optics described above assumes the incident illumination is plane-wave. In such a case the pattern of light produced by a grating does not depend upon the distance of the object, so long as the object is farther from the sensor than roughly 10 times the spatial scale of the sensor itself. As such, our sensor has extremely large effective depth of field, from roughly 1 mm to infinity.

The pattern of light produced by the diffraction grating strikes the CMOS photodetector matrix beneath and the signals are sent off chip for digital processing.

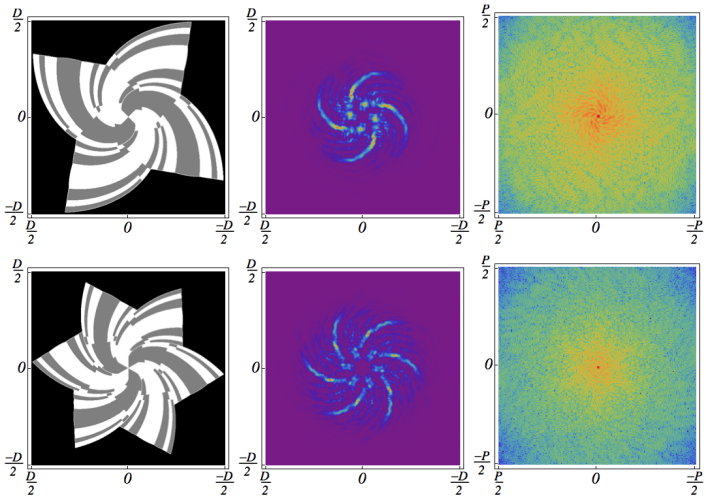

Fig. 5. The left column shows phase anti-symmetric spiral binary gratings, the middle column the point-spread function each produces (both figures of spatial extent $D \times D$, for some distance D). The right column shows the corresponding modulation transfer function (modulus of the Fourier transform) of extent $1/P \times 1/P$, where P is the pixel pitch and determines the Nyquist rate. The top row corresponds to four-fold chiral symmetry and the bottom row corresponds to six-fold chiral symmetry.

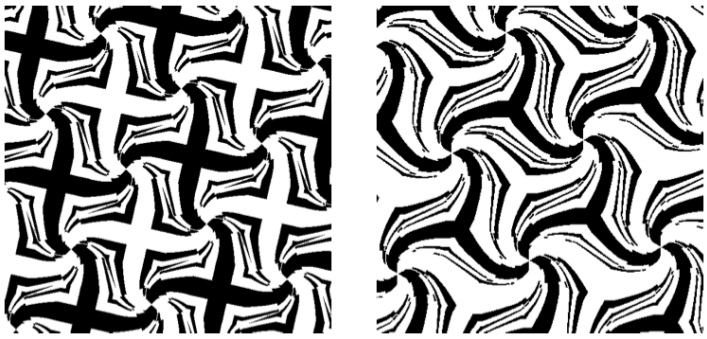

Fig. 6. The individual grating tiles of Fig. 5 can be packed to cover a photodetector matrix of arbitrary area.

C. Signal processing

Sensed signals in our sensor do not resemble an image in a camera obscura but must be processed to yield a digital image. We assume the overall forward imaging model is described by:

$$\mathbf{y} = \mathbf{A}\mathbf{x} + \mathbf{n}, \tag{1}$$

where $\mathbf{y}$ is the vector of photodetector pixel responses, $\mathbf{x}$ is a vector of inputs, $\mathbf{A}$ the matrix describing the linear transformation performed by the two-dimensional optical grating, and $\mathbf{n}$ is additive noise, which describes photodetector noise, Poisson photon statistics, quantization noise, etc. (Other models, such as simple multiplicative noise, could also be assumed.) We let both $\mathbf{x}$ and $\mathbf{n}$ be m-dimensional, $\mathbf{y}$ be n-dimensional, and hence $\mathbf{A}$ has dimensions $m \times n$.

The regularized least-square estimation problem—that is, the reconstruction of the image—can be expressed as finding the image $\hat{\mathbf{x}}$ that minimizes the error or cost function

$$\mathcal{C} = \|\mathbf{A}\hat{\mathbf{x}} - \mathbf{y}\|^2 + \|\mathbf{\Gamma}\hat{\mathbf{x}}\|^2, \tag{2}$$

where $\mathbf{\Gamma}$ weights the different components of $\hat{\mathbf{x}}$, for instance to accommodate differences prior probabilities of pixel values in the expected scenes. The image that minimizes the cost $\mathcal{C}$ in Equation 2 is [21]

$$\hat{\mathbf{x}} = \left(\mathbf{A}^t\mathbf{A} + \mathbf{\Gamma}^t\mathbf{\Gamma}\right)^{-1}\mathbf{A}^t\mathbf{y}. \tag{3}$$

In the special case that prior information about scene statistics implies that each component of $\hat{\mathbf{x}}$ should be penalized equally ($\mathbf{\Gamma} \propto \mathbf{I}$, the identity matrix), the solution can be written as

$$\hat{\mathbf{x}} = \left(\mathbf{A}^t\mathbf{A} + \gamma\mathbf{I}\right)^{-1}\mathbf{A}^t\mathbf{y}, \tag{4}$$

where γ is a scalar Tikhonov regularization parameter, whose optimal value depends upon the noise level [18], [22]. Cost functions other than that in Eq. 2 can be used as well, for instance those based on the *total variation* or *TV* norm of $\hat{\mathbf{x}}$, or on the L_1 norm, or on Bayesian prior information, or on weighted combinations of such penalty terms [23].

The computational burden of estimating the "best" image (in a sum-squared-error sense) compatible with the measured sensor signals $\mathbf{y}$ depends upon the particular form of the cost function $\mathcal{C}$. For the simple Tikhonov regularization in Eq. 4, before operation one precomputes the Moore-Penrose pseudo-inverse (possibly for different values of the regularization parameter)—an $\mathcal{O}(n^3)$ operation. Image estimation after signal capture is then a simple matrix multiply, an $\mathcal{O}(n^2)$ operation, easily parallelized to run at video rates in real-time on an FPGA or Graphics Processing Unit, if necessary. We note in passing that under certain circumstances (e.g., the function of the grating can be well approximated by a convolution operation), efficient Fourier estimation methods can be used instead, with an $\mathcal{O}(n \ln n)$ complexity.

Such estimation is well-conditioned and has higher fidelity when the modulation transfer function of the optical element contains no zeros, as is ensured by our special anti-symmetry phase gratings. Other reconstruction methods include inverse Wiener filtering and Bayesian methods such as Richardson-Lucy deconvolution, [24] each with computational complexities and fidelities that depend upon the accuracy of prior information about the source and other parameters. Figure 7 shows the estimation of an image through simple matrix inversion with Tikhonov regularization summarized in Eq. 4.

III. Simulation/design tools and methodology

Our sensor system design and analysis methods are based on a modular architecture comprising three software tools, all written in *Matlab* and executed on a large network of PCs:

- **Optics of phase gratings**: We simulate the interaction of light with gratings, for instance by finite-difference wave algorithms. These simulations predict the response of physical photodetector pixels to light incident at arbitrary angles.
- **CAD design of gratings and tiles**: We design gratings (spiral and otherwise) and their tilings. The output of our design is either *Matlab*-compatible files for optics simulations or *gdsII* for silicon grating manufacture.
- **Sensor signal processing**: We continue to write our own image reconstruction, signal estimation and pattern recognition software in *Matlab*, often using standard libraries of matrix operations.

We can employ *Perl* software wrappers for these components in order to efficiently design and model the system's end-to-end performance.

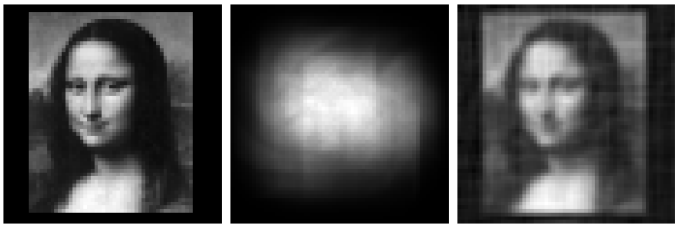

Fig. 7. Image sensing and computational reconstruction of Leonardo's *Mona Lisa* from a lensless phase anti-symmetric spiral phase grating sensor. (Left) The input image. (Middle) The simulated response on the photodetectors due to the six-fold grating in Fig. 5, and (right) the reconstruction by Eq. 4. This image estimate is of higher fidelity than the estimate based on traditional square-wave amplitude gratings and photodetector arrays of comparable number of pixels and overall noise level described in earlier work. [12]

IV. Hardware implementation

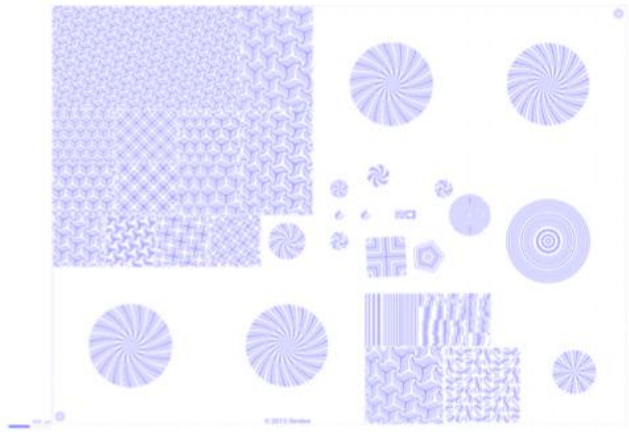

Fig. 8. The Ugoo silicate 5.5×4 mm contains 40 grating experiments. Tesselated for applications with lenses, as shown in Fig. 6. Fiducial marks at the lower-left and upper-right of the grid facilitate the estimation of the alignment of the grating with the underlying photodetector matrix.

Our experimental hardware implementation of PicoCam imagers and sensors is based on a single pixel-addressable 10 Mega-pixel sensor from Aptina, with a single large grating comprising 40 experiments (Fig. 8). The grating is made of a 50-μm-thick layer of silicate (known as Ugoo) affixed

to a 400-μm-thick glass substrate with grating steps of 1.5 μm, manufactured by Holographix, LLC. Figure 9 shows a micrograph of one portion of the full grating. Input images are presented on an LCD display under computer control, and signals are read directly from the Aptina sensor and processed on a PC.

Experimental calibration of the sensor and experimental verification of the above theory is in progress and will be presented separately.

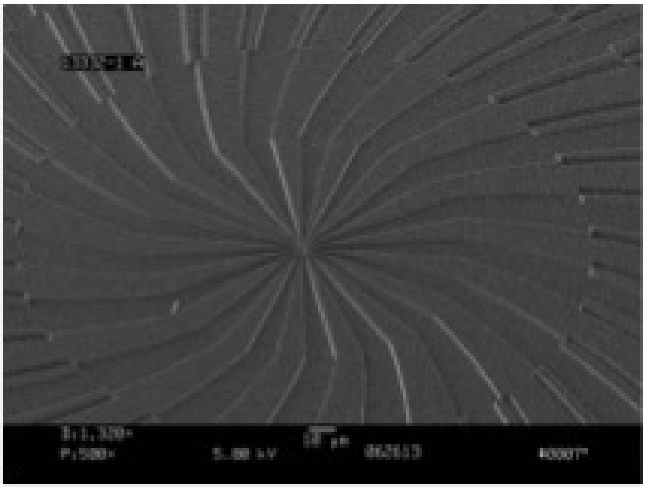

Fig. 9. Circular versions of the left column of Fig. 5.

V. Applications

There are many promising applications for our sensors which fall into a number of general categories. A small but important subset of such categories follows.

A. Imaging

The ultra-miniature size of our imagers and sensors make them especially appropriate for medical and industrial endoscopy as well as traditional and novel mobile computing devices. There are many surveillance applications that would profit from low- to mid-level resolutions as well. Because these sensors are so inexpensive (in bulk)—each less expensive than a single frame of 35-mm photographic film—they could find application in a number of one-use imaging scenarios arising in military theaters, hazardous industrial conditions (crash tests) and natural environments [25], [26]. Another general area is inexpensive mobile medical imaging and sensing. A key design decision is where the signal processing should be implemented—close to the sensor itself, or instead on a host machine, possibly delayed from the signal capture.

B. Motion estimation

The optical gratings and signal processing algorithms can be tailored to broad image sensing applications such as occupancy detection for controlled lighting, motion (motion-activated devices), visual looming (pre-impact automotive airbag deployment), interactive toys, and numerous applications in support of the Internet of Things [27].

C. Pattern recognition

These sensors can extract informative visual information for pattern recognition applications, such as face detection (authentication), one-dimensional barcode and two-dimensional QR code reading, gesture recognition and many others. Of course, the signal processing is then based on principles of pattern recognition appropriate for the task at hand [28].

VI. Conclusion

We have designed and verified through full end-to-end system simulation a new class of lensless computational imagers based on phase anti-symmetric spiral gratings. We have built the components and are moving towards full hardware characterization of gratings and verification of imaging functionality. These imagers promise to be smaller (lower physical volume) than any existing lens-based imagers of comparable resolution, very inexpensive, and customizable to both imaging and a wide range of sensing and image measurement tasks.

Practical fielded applications will lead to many interesting problems in efficient application-specific algorithms, either on special-purpose ASICs, on highly parallel graphics processor units (GPUs), or on general-purpose central processor units (CPUs). Networks of such sensors highlight several problems and opportunities in power usage and bandwidth optimization.

Acknowledgment

We thank Thomas Vogelsang and Michael Ching for helpful comments.

References

[1] T. Gustavson, *Camera: A history of photography from Daguerreotype to digital*. New York, NY: Sterling Publishing Co., 2009.

[2] D. Wooters and T. Mulligan, *A history of photography—from 1839 to the present*. New York, NY: Taschen, 2005.

[3] W. T. Cathey and E. R. Dowski, Jr., "A new paradigm for imaging systems," *Applied Optics*, vol. 42, no. 29, pp. 6080–6092, 2002.

[4] D. G. Stork and M. D. Robinson, "Theoretical foundations of joint design of electro-optical imaging systems," *Applied Optics*, vol. 47, no. 10, pp. B64–75, 2008.

[5] E. H. Adelson and J. Y. Wang, "Single lens stereo with a plenoptic camera," *IEEE Transactions on Pattern Analysis and Machine Intelligence*, vol. 14, no. 2, pp. 99–106, 1992.

[6] A. Levin, R. Fergus, F. Durand, and W. T. Freeman, "Image and depth from a conventional camera with a coded aperture," *ACM Transactions on Graphics*, vol. 26, no. 3, pp. 70:1–70:9, 2007.

[7] D. L. Marks, D. S. Kittle, H. S. Son, S. H. Youn, S. D. Feller, J. Kim, D. J. Brady, D. R. Golish, E. M. Vera, M. E. Gehm, R. A. Stack, E. J. Tremblay, and J. E. Ford, "Gigapixel imaging with the AWARE multiscale camera," *Optics and Photonics News*, vol. 23, no. 12, p. 31, 2012.

[8] D. L. Donoho, "Compressed sensing," *IEEE Transactions on Information Theory*, vol. 52, no. 4, pp. 1289–1306, 2006.

[9] M. F. Duarte, M. A. Davenport, D. Takhar, J. N. Laska, T. Sun, K. F. Kelly, and R. G. Baraniuk, "Single-pixel imaging via compressive sampling," *IEEE Signal Processing Magazine*, vol. 25, no. 2, pp. 83–91, 2008.

[10] J. M. Kahn, R. H. Katz, and K. S. J. Pister, "Next century challenges: Mobile networking for 'Smart Dust'," in *Proceedings of the 5th Annual ACM/IEEE International Conference on Mobile Computing and Networking (MobiComm 99)*, 1999, pp. 271–278.

[11] P. R. Gill, C. Lee, D.-G. Lee, A. Wang, and A. Molnar, "A microscale camera using direct Fourier-domain scene capture," *Optics Letters*, vol. 36, no. 15, pp. 2949–2951, 2011.

[12] P. R. Gill, C. Lee, S. Sivaramakrishnan, and A. Molnar, "Robustness of planar Fourier capture arrays to colour changes and lost pixels," *Journal of Instrumentation*, vol. 7, pp. C01–61, 2012.

[13] A. Wang and A. Molnar, "A light-field image sensor in 180 nm CMOS," *IEEE Journal of Solid-State Circuits*, vol. 47, no. 1, pp. 257–271, 2012.

[14] A. Wang, P. R. Gill, and A. Molnar, "Light field image sensors based on the Talbot effect," *Applied Optics*, vol. 48, no. 31, pp. 5897–5905, 2009.

[15] D. G. Stork and P. R. Gill, "Lensless ultra-miniature CMOS computational imagers and sensors," in *SensorComm 2013*, Barcelona, Spain, 2013, pp. 186–190.

[16] S. Sivaramakrishnan, A. Wang, P. R. Gill, and A. Molnar, "Enhanced angle sensitive pixels for light field imaging," in *IEEE International Electron Devices Meeting (IEDM)*, 2011, pp. 8.6.1–8.6.4.

[17] C. Peroz, S. Dhuey, A. Goltsov, M. Volger, B. Harteneck, I. Ivonin, A. Bugrov, S. Cabrini, S. Babin, and V. Yankov, "Digital spectrometer-on-chip fabricated by step and repeat nanoimprint lithography on pre-spin coated films," *Microelectronic Engineering*, vol. 88, no. 8, pp. 2092–2095, 2011.

[18] P. R. Gill and D. G. Stork, "Lensless ultra-miniature imagers using odd-symmetry spiral phase gratings," in *Optical Society of America Sensors Congress*, 2013.

[19] R. L. Morrison, "Symmetries that simplify the design of spot array phase gratings," *Journal of the Optical Society of America A*, vol. 9, no. 3, pp. 464–471, 1992.

[20] P. R. Gill, "Odd-symmetry phase gratings produce optical nulls uniquely insensitive to wavelength and depth," *Optics Letters*, vol. 38, no. 12, pp. 2074–2076, 2013.

[21] R. Penrose, "On the best approximate solution of linear matrix equations," *Proceedings of the Cambridge Philosophical Society*, vol. 52, pp. 17–19, 1956.

[22] D. G. Manolakis, V. K. Ingle, and S. M. Kogon, *Statistical and adaptive signal processing: Spectral estimation, signal modeling, adaptive filtering and array processing*. Norwood, MA: Artech, 2005.

[23] T. Hastie, R. Tibshirani, and J. Friedman, *The Elements of Statistical Learning: Data Mining, Inference, and Prediction*, 2nd ed. New York, NY: Springer, 2009.

[24] D. A. Fish, A. M. Brinicombe, E. R. Pike, and J. G. Walker, "Blind deconvolution by means of the Richardson-Lucy algorithm," *Journal of the Optical Society of America A*, vol. 12, no. 1, pp. 58–65, 1995.

[25] P. R. Gill, "Disposable sensors: Computational imaging and sensing supports one-time use devices," in *Proceedings of the Trillion Sensor Summit*, Stanford University, 2013, p. 115.

[26] D. G. Stork, "Disposable ultra-miniature sensors: Computational imaging for one-time use devices," in *Proceedings of the Trillion Sensor Summit Tokyo*, J. Bryzdek and A. P. Pisano, Eds., Tokyo, 2014 (in press).

[27] H. Chaouchi, Ed., *The Internet of Things: Connecting objects*. New York, NY: Wiley, 2010.

[28] R. O. Duda, P. E. Hart, and D. G. Stork, *Pattern Classification*, 2nd ed. New York, NY: Wiley, 2001.